Lab on a Chip

PAPER

View Article Online
View Journal

Cite this: DOI: 10.1039/c5lc01515d

A microfluidic method for dopamine uptake measurements in dopaminergic neurons†

Yue Yu,[ab] Mohtashim H. Shamsi,‡[bc] Dimitar L. Krastev,[d] Michael D. M. Dryden,[c] Yen Leung[b] and Aaron R. Wheeler*[abc]

Received 10th December 2015,
Accepted 18th December 2015

DOI: 10.1039/c5lc01515d

www.rsc.org/loc

Dopamine (DA) is a classical neurotransmitter and dysfunction in its synaptic handling underlies many neurological disorders, including addiction, depression, and neurodegeneration. A key to understanding DA dysfunction is the accurate measurement of dopamine uptake by dopaminergic neurons. Current methods that allow for the analysis of dopamine uptake rely on standard multiwell-plate based ELISA, or on carbon-fibre microelectrodes used in *in vivo* recording techniques. The former suffers from challenges associated with automation and analyte degradation, while the latter has low throughput and is not ideal for laboratory screening. In response to these challenges, we introduce a digital microfluidic platform to evaluate dopamine homeostasis in *in vitro* neuron culture. The method features voltammetric dopamine sensors with limit of detection of 30 nM integrated with cell culture sites for multi-day neuron culture and differentiation. We demonstrate the utility of the new technique for DA uptake assays featuring in-line culture and analysis, with a determination of uptake of approximately ~32 fmol in 10 min per virtual microwell (each containing ~200 differentiated SH-SY5Y cells). We propose that future generations of this technique will be useful for drug discovery for neurodegenerative disease as well as for a wide range of applications that would benefit from integrated cell culture and electroanalysis.

Introduction

Dopamine (DA) is a classical small-molecule neurotransmitter. In a typical dopaminergic neurotransmission event, DA molecules are exocytosed from a presynaptic neuron, where they diffuse across the synaptic cleft to bind an appropriate receptor on the postsynaptic neuron. DA is then cleared from the synapse through a number of mechanisms including passive diffusion, receptor internalization and transporter uptake. Defects in DA clearance and regulation are implicated in a host of diseases such as attention deficit hyperactive disorder, depression, addiction, and Parkinson's disease (PD).[1,2] For example, in some cases of PD, the dopamine transporter interacts with parkin and synuclein,[3–6] forming anomalous constructs which decrease the rate of dopamine clearance. Currently, the most common technique used to evaluate these phenomena is the dopamine uptake assay, in which neurons are incubated with exogenous dopamine, after which the amount of dopamine found in cell lysate or remaining in the extracellular media is measured as a function of time.[1,4,7–9]

Dopamine uptake assays are often implemented *in vitro* in multiwell plates, which allows for convenient screening of molecular species to identify effectors of dopamine clearance. A popular model for these experiments is the SH-SY5Y cell line, which differentiates into a functional dopaminergic neuron model when incubated with retinoic acid (RA) and 12-*O*-tetradecanoylphorbol-13-acetate (TPA).[10] The amount of dopamine uptake by SH-SY5Y or other dopaminergic neurons is typically determined using immunochemistry (*e.g.*, Western blot or ELISAs) or radioisotopes.[1,10] This requires tedious steps involving transfer of analytes between vessels and instruments, which may lead to data loss and variability. This is particularly problematic for DA given its propensity to become oxidized when exposed to air.[11,12] An alternate technique (which is often applied in *in vivo* studies[13,14]) is the use of microelectrodes and amperometry to measure dopamine directly in the extracellular milieu. While this technique has become an important tool for correlation of dopamine release and uptake with whole-organism behaviour, two key issues hold back its adoption for *in vitro* biochemical studies:

[a] *Institute for Biomaterials and Biomedical Engineering, University of Toronto, 164 College St, Toronto, ON, M5s 3G9, Canada.*
E-mail: aaron.wheeler@utoronto.ca; Fax: 416 946 3865; Tel: 416 946 3864
[b] *Donnelly Centre for Cellular and Biomolecular Research, 160 College St., Toronto, ON, M5S 3E1, Canada*
[c] *Department of Chemistry, University of Toronto, 80 St Georg St., Toronto, ON, M5S 3H6, Canada*
[d] *Department of Human Biology, University of Toronto, 300 Huron Street, Toronto, ON, M5S 3J6, Canada*
† Electronic supplementary information (ESI) available. See DOI: 10.1039/c5lc01515d
‡ Current Address: Department of Chemistry and Biochemistry, Southern Illinois University at Carbondale, 1245 Lincoln drive, Carbondale, IL, 62901, USA.

(1) the method uses fragile (and typically home-made) pulled-capillary carbon fiber electrodes as the transducer, and (2) usage of these electrodes requires 3D micromanipulators and a microscopy stage, limiting the throughput for screening.

Here, we report a potential solution to the problems described above, relying on digital microfluidics[15] (DMF) to integrate two functions: (a) multi-day neuronal cell culture and (b) quantitative electroanalyis of dopamine. In DMF, discrete droplets are manipulated across an open surface, sandwiched between two parallel glass plates (top and bottom). The top plate is coated with transparent, conductive indium tin oxide (ITO) acting as a DMF counter-electrode, and the bottom plate is a patterned array of driving electrodes coated with a dielectric layer. Towards application (a), DMF has proven useful[16] for automating many of the tedious steps involved in *in vitro* mammalian cell culture[17–23] but (unlike methods relying on microchannels or micropatterning, which have been used extensively for applications in neuroscience[24–31]), DMF has never before been applied to neuron cell culture and analysis. Towards application (b), DMF has been combined with electroanalysis,[32–36] and was recently applied to detecting dopamine.[33] However DMF has never been used to integrate cell culture with electroanalysis, and in fact, we are unaware of any report of DMF cell culture being integrated with any type of chemical sensor. Multi-day cell culture and electroanalysis have disparate (and in some cases, contraindicated) requirements, but after a significant amount of design and trial and error, the two functions proved to be compatible, as described here.

The new technique introduced here is a comprehensive tool, allowing for automated multiday dopaminergic neuron cell culture and differentiation combined with in-line quantification of dopamine using a custom, integrated voltammetric sensor. The new system was validated by application to the evaluation of dopamine uptake in differentiated SH-SY5Y cells. We propose that these and related techniques will be applicable to a wide range of problems in neuroscience and beyond that would benefit from integrated in-line cell culture and electroanalysis.

Materials and methods

Unless otherwise specified, reagents were purchased from Sigma Chemical (Oakville, ON, Canada) or Fisher Scientific Canada (Ottawa, ON, Canada). Fluorescent dyes and cell culture reagents were purchased from Life Technologies (Burlington, ON, Canada). Antibodies were purchased from Abcam (Ab) (Cambridge, UK) and Cell Signaling Technologies (CST) (Danvers, MA, USA). A stock solution of dopamine was prepared by dissolving 1.90 mg of dopamine in 10 mL of 1× phosphate buffered saline (PBS) buffer (pH = 7.4) to a final concentration of 1 mM. Two sets of serial dilutions of dopamine were prepared in PBS: (a) 500, 100, 50, 10, 5, 1 μM, and (b) 500, 100, 50, 10 nM from the stock solution. All solutions used in DMF experiments contained a surfactant additive; when not explicitly listed, the surfactant was 0.05% Pluronic F68.

Macroscale cell culture

SH-SY5Y and MDA-MB-231 cells were acquired from ATCC (Manassas, VA) and cultured in T25 flasks in a humidified incubator at 37 °C with 5% CO_2. SH-SY5Y cells were grown in 1 : 1 DMEM : F12 supplemented with 10% FBS and 100 U mL^{-1} penicillin/streptomycin. MDA-MB-231 cells were cultured in DMEM supplemented with 10% FBS and 100 U mL^{-1} penicillin/streptomycin. Cellular protein content was determined with the Lowry method according to manufacturer's instructions (TP0300, Sigma, Oakville, Canada), measuring the absorbance at 570 nm on a Pherastar multi-well plate reader (BMG Labtech, Offenburg, Germany).

Fabrication of DMF bottom plates

DMF bottom plates were fabricated in the cleanroom facilities of the Toronto Nanofabrication Centre (TNFC), University of Toronto. Patterned chromium-on-glass substrates were coated with Parylene-C and Teflon AF as described previously.[37] Briefly, the design features 80 chromium actuation electrodes (2 × 2 mm), connected to 8 reservoir and 4 waste electrodes, all coated with ~15 μm parylene C (Specialty Coating Systems, Indianapolis, Indiana, USA) and ~100 nm Teflon AF (Dupont, Wilmington, Delaware, USA).

Fabrication of DMF top plates

ITO coated glass substrates (Delta Technologies Ltd, Stillwater, MN) were processed in two photolithography stages to create DMF top plates with integrated electroanalytical electrodes and designated areas for neuron culture. In the first stage, ITO was patterned and etched as described previously,[32] resulting in five electrically isolated electrodes. Four of the electrodes comprised two identical two-electrode electrochemical cells (in the center of the substrate), and the fifth electrode occupied an irregular area covering the remainder of the substrate (and served as the DMF counter-electrode). Each electrochemical cell featured one working electrode (WE) with a surface area of 1.19 mm^2, surrounded by a circular counter/pseudoreference electrode (CE/RE), which was 11.9 mm^2 (with a 10 μm gap between each WE-CE/RE pair). Working electrodes were patterned either in the shape of an eight-armed star (arm-width: 100 μm, arm-length: 0.95 mm), a four-armed cross (arm-width: 200 μm, arm-length: 0.95 mm), a line (width: 310 μm, length: 3.84 mm), or a solid circle (radius: 0.61 mm). Each of the electrochemical cell electrodes was connected by a thin wire (width: 100 μm) to a dedicated square shaped contact pad (10 mm × 10 mm) located on the edge of the substrate.

The second photolithography stage was adapted from a protocol described previously[21] to form hydrophilic liftoff spots on Teflon AF-coated DMF top plates. Briefly, substrates from stage one (above) were cleaned, spin coated with photoresist (S1811, Dow Chemicals, Midland, Michigan, US) and

exposed to UV light through a photomask. After developing, Teflon AF was spin-coated at 4000 RPM and post baked at 175 °C for 5 minutes before immersion in acetone to lift-off four circular 2 mm dia. apertures through the Teflon AF. Then, the substrate was baked successively on a hot plate at 260 °C and 170 °C for 10 minutes each. When complete, the final substrate had a global coating of Teflon AF, with four 2 mm dia. circular (open) apertures, two of which were centered over the electrochemical cells (defined in the first photolithography stage, above), and two of which were over the DMF counter-electrode (dedicated for neuron culture).

Two plate DMF device assembly and operation

Top and bottom plates were assembled with 150 μm thick spacers formed from double-sided tape, such that unit droplets (covering one actuation electrode) were 600 nL. Droplets were actuated by applying 100 V_{RMS} electric potentials between DMF actuation electrodes (on the bottom plate) and counter-electrode (on the top plate), controlled and managed using the open-source DropBot system as described previously.[38] In all droplet manipulation procedures, the device was oriented with the top plate on "top," but in all incubation procedures, the device was inverted, with the top plate on the "bottom."

On-chip cell culture and differentiation

24 h prior to beginning experiments using DMF devices, the hydrophilic liftoff areas on top-plates designated for cell culture were incubated overnight with 10 μM poly-D-lysine (PDL) in double distilled water. 3 h before cell seeding, the top plates were washed three times with sterile water and allowed to air dry in a biosafety cabinet. SH-SY5Y cells that were destined to be differentiated into neurons were grown to 65% confluence in a T25 flask, detached with 0.05% Trypsin in EDTA and resuspended at 4 million cells per mL in retinoic acid (RA) differentiation medium [1 : 1 DMEM : F12 supplemented with 1% FBS, 100 U mL^{-1} penicillin/streptomycin, 20 μM all-trans retinoic acid (RA), and 0.05% Pluronic F68]. A 10 μL aliquot of the resuspended cells was loaded into a reservoir on the assembled DMF device and two unit droplets were dispensed, merged, and then actuated across one of the PDL-coated hydrophilic sites to passively dispense a ~470 nL virtual microwell to seed the cells (and the remainder of the solution was driven to waste). 5 hours after seeding, fresh RA differentiation medium was loaded into the device and a unit droplet was driven across the hydrophilic site to replace the spent media in the virtual microwell with fresh medium. This was repeated every 24 hours for 3 days, after which the medium was switched to 12-*O*-tetradecanoylphorbol-13-acetate (TPA) differentiation medium (identical to RA differentiation medium but supplemented with 10 μM TPA instead of RA). The 24 h media replacements were continued for another 3 days. MDA-MB-231 cells and SH-SY5Y cells not destined to be differentiated were prepared similarly, but were suspended in (and replenished every 24 h in) MDA-MB-231 media or standard SH-SY5Y media. During all times in which droplets were not being manipulated, devices were inverted and kept in a humidified incubator at 37 °C with 5% CO_2.

Immunocytochemistry on DMF

Day 6 differentiated SH-SY5Y cells grown on PDL-coated hydrophilic sites in DMF devices were evaluated by a technique known as digital microfluidic immunocytochemistry in single cells[22] (DISC) in a 10-step procedure. Briefly, (1) cells were fixed by dispensing and driving a unit droplet of 4% paraformaldehyde in PBS with 0.05% Pluronic F-68 across the hydrophilic site. (2) The cells were washed by dispensing and driving two unit droplets of PBS containing 0.05% Brij-35 across the site (in series), and (3) they were permeabilized by dispensing and driving a unit droplet of 0.2% Tween 20 in PBS across the site. (4) Step two was repeated. (5) Primary antibodies were delivered to the fixed, permeabilized cells by dispensing and driving a unit droplet containing one or more of rabbit anti-beta 3 tubulin (ab18207 diluted 1 : 800), or murine anti-mitochondrial (ab3298 diluted 1 : 20) in 1% non-fat dry milk in PBS supplemented with 0.05% Brij-35 across the hydrophilic site. (6) Step two was repeated again, and (7) step five was repeated with secondary antibodies including Alexa Fluor 647 conjugated anti-mouse (CST#4410 diluted 1 : 600) or Alexa Fluor 555 conjugated anti-rabbit (CST#4413 diluted 1 : 1200). (8) The top plate was detached from the DMF device and immersed in 0.1% PBS with 0.05% Tween 20, followed by (9) washing in distilled water, and subsequently (10) the substrate was allowed to air dry.

The dried substrate was evaluated by whole-well microscopy using an Axon Instruments (Sunnyvale, CA, USA) Genepix 4000B microarray plate reader and an Olympus (Tokyo, Japan) IX71 microscope with a BH2-RFL-T3 fluorescent source. Images were white-balanced and stitched together using Affinity Designer (Serif, Nottingham, England.)

Electrochemical analysis

Electrochemical analysis was performed using an Emstat potentiostat (PalmSens, BV, Utrecht, the Netherlands). As an initial characterization, each WE geometry (circle, line, cross, star) was incubated with 200 μM dichlorotris(1,10-phenanthroline)ruthenium(II) in 1× PBS and cyclic voltammagrams (CVs) were collected at 0.1 V s^{-1}, scanning from −1 V to 1.5 V. The star-shaped WE geometry was also characterized by collecting CVs of 1 mM 1 : 1 potassium hexacyanoferrate(II) : potassium hexacyanoferrate(III) in 1× PBS buffer at scan rates of 2, 1, 0.5, 0.25, 0.1 V s^{-1}, scanning from −1.2 V to 1.2 V. For each condition, the final five scans were recorded, and the average cathodic and anodic peak currents were calculated for analysis.

An voltammetric calibration curve for dopamine was generated on-chip by performing cyclic voltammetry on unit droplets containing dopamine (10 μM to 10 nM in PBS) at 100 mV s^{-1}, scanning from −0.9 V to +0.9 V (on devices with

the star-shaped WE). Ten scans were collected at each concentration, and the average cathodic peak currents at 720 mV from the final five scans were recorded for analysis. The cathodic peak was plotted as a function of concentration and fitted with a linear least squares regression. The limit of detection (LOD) was defined as the concentration (from the regression) corresponding to the average blank signal plus three times the standard deviation of the blank signal.

Dopamine uptake assay

Day-6 differentiated SH-SY5Y cells were washed by dispensing and driving two unit droplets (in series) containing PBS (pre-warmed to 37 °C) across the virtual microwell (moving the droplet remainder to the waste reservoir). A droplet of PBS containing 1 μM dopamine (pre-warmed to 37 °C) was then driven across the virtual microwell, followed by incubation for 10 minutes in the 37 °C incubator. After incubation, a fresh unit droplet of differentiation media was dispensed and driven across the microwells to collect the spent dopamine solution. The droplet containing spent-solution was driven to the electroanalytical cell for measurement using the procedure described above. The procedure above was repeated for PDL-coated microwells with no cells, as well as PDL-coated microwells bearing day-2 undifferentiated SH-SY5Y cells or day-2 MDA-MB-231 cells. In addition, the procedure was repeated for day-6 differentiated SH-SY5Y cells with PBS not containing dopamine. Statistical significance was evaluated by student's *t*-test.

Supplementary methods

Supplementary methods describing simulations of diffusion over working electrodes, as well as experiments evaluating SH-SY5Y cell differentiation and analyte transfer efficiency are described in the online supplementary materials.

Results and discussion

Device and detector

The overall goal for this work was to develop an integrated system capable of multi-day neuronal cell culture with in-line electroanalysis of dopamine uptake. As a first step towards this goal, a new device architecture was designed combining two previously published techniques: DMF top-plates modified with hydrophilic liftoff areas for *in vitro* adherent cell culture in so-called "virtual microwells"[21] and DMF top-plates modified with electrochemical cells for quantitative analysis by amperometry.[32] We call the new system an Electroanalysis-Microwell DMF top plate (or "EM-top plate"). The EM-top plate was designed to enable rapid, integrated transfer of reagents between cell culture zones and detectors, thus minimizing the dopamine auto-oxidation[11,12] that plagues conventional dopamine uptake assays.

Fig. 1a depicts an EM-top plate patterned with three distinct regions: (1) a hydrophobic Teflon AF-coated DMF counter-electrode for droplet actuation, which covers most of the top plate, (2) two hydrophilic Teflon AF lift-off spots for electroanalysis, and (3) two hydrophilic Teflon AF lift-off spots for cell culture. Each culture site is positioned adjacent to an electroanalytical cell (4 mm edge-to-edge). The magnified view of Fig. 1a demonstrates that the electroanalytical cell comprises a two-electrode system: an ITO working electrode (WE, red) and an ITO counter/pseudoreference electrode (CE/RE, blue). Each cell culture site is coated with poly-D-lysine (PDL, green).

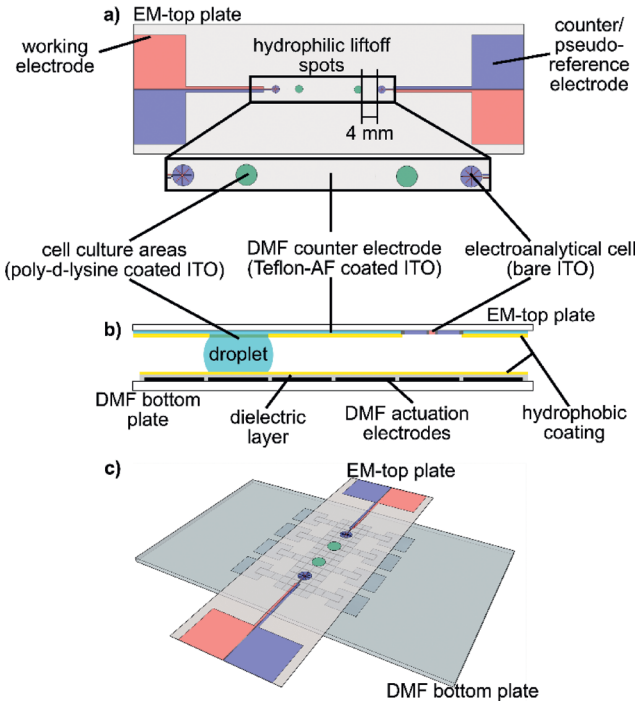

Fig. 1 Digital microfluidic (DMF) device for integrated neuronal cell culture and electroanalysis. a) Top view schematic of the new Electroanalysis-Microwell DMF top plate (EM-top plate). The conductive ITO is patterned into 5 electrically isolated zones: 2× working electrodes (red), 2× counter/pseudoreference electrodes (blue), and one large, irregular DMF counter electrode. A magnified view (below) shows the composition of four hydrophilic liftoff spots (*i.e.*, apertures through the Teflon AF): 2× electrochemical cell (red/blue – bare ITO) and 2× cell culture areas (green – ITO coated with poly-D-lysine). b) Side view schematic of a DMF device bearing a droplet positioned on one of the cell culture areas. c) Isometric view of the assembled device.

Fig. 1b shows a side view of an EM-top plate assembled in a DMF device. In DMF, droplets sandwiched between top and bottom plates are manipulated by applying potentials between driving electrodes on the bottom plate and a ground electrode on the top plate. As described previously,[21] the Teflon AF liftoff sites on the top plate (either for cell culture or for electroanalysis) facilitate a phenomenon called "passive dispensing" in which a two-unit droplet (in this case ~1200 nL) crosses a hydrophilic region, spontaneously forming a virtual microwell (in this case ~470 nL). After initial formation of the virtual microwell, passing a single unit droplet across the site is sufficient to sweep the microwell's contents away for analysis or to waste.

The final design of the system used here (Fig. 1) was determined after several iterations, striving to balance numerous requirements. First, because adherent cell culture is (by its nature) destructive to surfaces, the devices cannot be re-used for multiple experiments, making it critical that the fabrication protocol be as straightforward as possible (to allow for rapid generation of many devices for replicates). Thus, in contrast to all previous DMF-electroanalysis devices,[32–36] the electroanalysis electrodes used here were formed from unmodified ITO rather than metal. This is advantageous because ITO is already incorporated (by design) as the DMF counter-electrode; only minor additions to the conventional fabrication steps are necessary to integrate the electroanalytical cell. Likewise, given the complexity of the overall device design (Fig. 1), it was desirable to use a simple two-electrode electrochemical cell format[32] (incorporating one WE and one CE/RE) rather than the more common three-electrode cell format.[33–36] Second, despite the non-standard material and format imposed on the new detector (above), it was critical that it be stable, precise, and have sensitivity sufficient to detect changes in dopamine concentration on the order of ~nM.

The criteria for the new electroanalytical cell (above) posed some design challenges. For example, it is well known[39] that to avoid the possibility of potential drift inherent in two-electrode cells, the CE/RE must have an area ≥10× larger than the WE area. A problem with this strategy is solution resistance – if the electrode geometries are not carefully considered, a large CE/RE area : WE area ratio can result in large distances between the electrodes (and/or samples that lie primarily over the CE/RE), which can exacerbate the problem of uncompensated solution resistance, reducing sensor efficiency and increasing the measurement error. To evaluate this phenomenon and optimize detector performance, the WEs used in this study were formed bearing four different geometries: i) round, ii) line, iii) cross, and iv) star, all embedded as inserts into the larger CE/RE (Fig. 2a). These cells were constructed with consistent size ratio of 10 : 1 between CE/RE and WE, where the area of WE = 1.19 mm^2. Photomicrographs of the four WE geometries tested here are pictured in Fig. 2b shows representative cyclic voltammograms (CVs) generated for each of the geometries using a common electroanalysis test-mixture, dichlorotris(1,10-phenanthroline)-ruthenium(II). Fig. 2c compares the oxidation peak currents (blue squares, referenced to the left axis) for this analyte for each of the four WE geometries at 1.3 V. It is evident that an increased WE perimeter, ranging from 1.83 mm for the circular WE (the geometry most similar to conventional screen-printed electrochemical cells) to 11.85 mm for the star shaped WE, results in increased signal and reduced noise; the star-shaped electrode was used for all subsequent experiments.

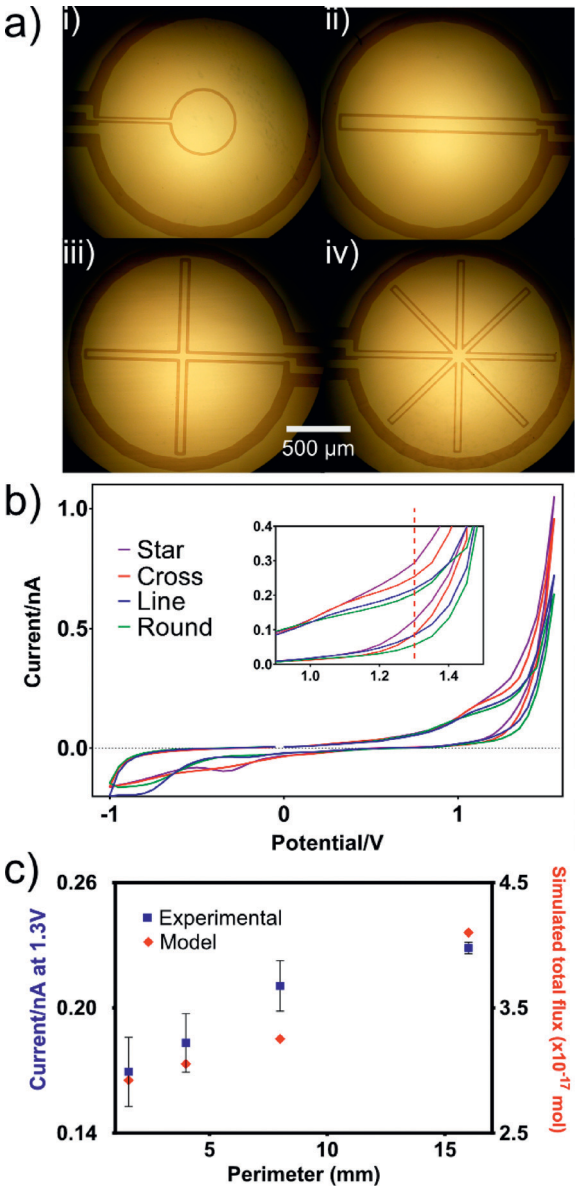

Fig. 2 Characterization of working electrode (WE) geometries in EM-top plates. a) Micrographs of WEs formed with i) round, ii) line, iii) cross, and iv) star geometries, scale bar is 500 μm. b) Representative cyclic voltammograms (CVs) of 200 μM dichlorotris(1,10-phenanthroline)ruthenium(II) in 1× PBS buffer (pH 7.4), recorded at 1 V s^{-1} for the star (purple), cross (red), line (blue), and round (green) WE geometries. The inset is a magnified region around 1.3 V. c) Comparison of measured peak current measured at 1.3 V (blue squares, left axis) and simulated total flux for 10 s (red diamonds, right axis; see online supplementary information for details) as a function of WE perimeter, increasing from the round geometry on the left, to the star on the right. For the current measurements, error bars represent ±1 standard deviation (S.D.) for n = 5 The star-shaped WE geometry had the greatest signal and lowest variance, and thus was used for all subsequent experiments.

We attribute the effect of WE perimeter on signal to improved access for the analyte diffusing onto the WE during the measurement period. A similar trend can be found by simulating the diffusion of analyte onto regions with geometries that match the working electrodes (Fig. S1 in the online ESI†). The total flux of analyte onto each geometry in a 10 s period is plotted for each geometry (red diamonds, referenced to the right axis) in Fig. 2c. Note that the

phenomenon observed here (increasing perimeter of the working electrode to increase signal strength) is fundamentally the same as that established by microband electrodes which are commonly used and have been characterized in detail.[39]

All-ITO electroanalytical cells are rare; thus, the star-shaped ITO *vs.* ITO electroanalytical cell was further characterized for reversibility and stability by recording cyclic voltammograms of ferri/ferrocyanide mixtures at scan rates of 0.1–2 V s^{-1}. As shown in Fig. 3a, the peak separation was found to be ~1.8 V, which is different than the ideal case because of the uncompensated solution and electrode resistance (a consequence of thin wires and the relatively low conductivity of ITO). Note that this has negligible effects on the sensitivity of the system because the dopamine measurements generate currents in the ~nA range, which causes little electrode polarization. More importantly, Fig. 3b shows a linear relationship between the peak current and the square root of the scan rate as predicted by the Randles–Sevcik equation,[39] $i_p = (2.69 \times 10^5)AC_iD^{1/2}v^{1/2}n^{3/2}$, where i_p is peak current, A is the area of the WE, C_i is the concentration of the electroactive species, D is the diffusion coefficient, and v is the scan rate. Taken together, the electrochemical characterizations in Fig. 2 and 3 confirm the ability of the new ITO *vs.* ITO two-electrode electroanalytical cell to provide a platform with a reasonable potential window, as well as a stable and measurable electrochemical current signal in the nA scale.

Voltammetry has been employed for *in vivo* dopamine detection,[13,14,40] and while there have been reports of dopamine detection on metal-coated ITO surfaces,[33,40] we are not aware

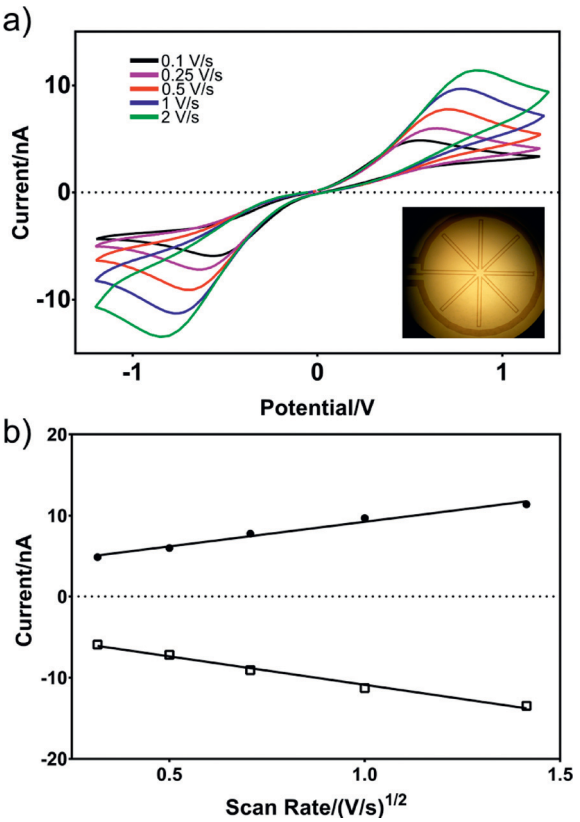

Fig. 3 Characterization of reversibility for EM-top plates bearing star-shaped WEs. a) CVs of 1 mM 1:1 potassium hexacyanoferrate(II): potassium hexacyanoferrate(III) in 1× PBS at scan rates of 0.1 (black), 0.25 (purple), 0.5 (red), 1 (blue), and 2 (green) V s^{-1}. Inset: photograph of star shaped electrode. b) Randles–Sevcik plot of anodic (●) and cathodic (○) peak currents as a function of the square root of scan rate.

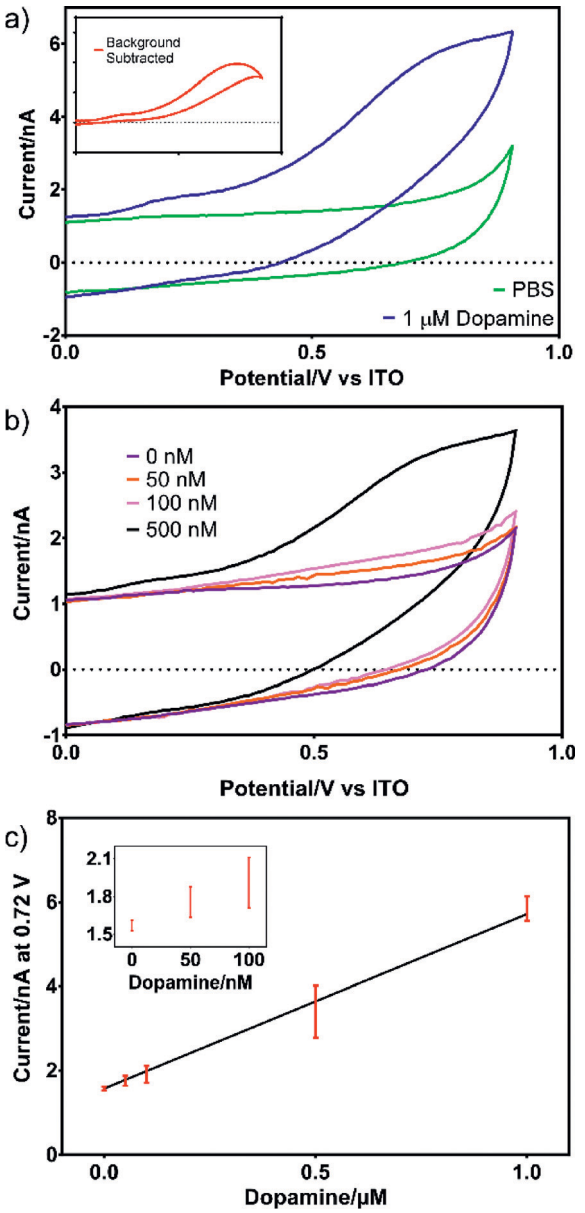

Fig. 4 Electrochemical analysis of dopamine standards in PBS using the EM-top plate. a) Representative CVs of 1 μM dopamine solution (blue) and background buffer, PBS (green). Inset: CV of background-subtracted trace (red), showing the oxidative peak at 0.72 V. b) Representative CVs of DA at 50 nM (orange), 100 nM (pink), 500 nM (black), and PBS (purple). c) Calibration curve generated by measuring the currents at 0.72 V for standards ranging from 0 nM to 1 μM DA. Error bars represent ±1 S.D. for n = 50. The limit of detection (defined as the concentration corresponding to the blank signal plus 3× the standard deviation of the blank) was determined to be 30 nM. The inset is a magnified view of the low end of the curve.

of any previous dopamine analyses carried out using bare ITO *vs.* ITO electrodes. Fig. 4a shows a representative CV of 1 μM dopamine in PBS collected using an EM-top plate. Since dopamine oxidation is a two-electron process, two oxidation peaks are observed, at 0.3 V and 0.72 V, confirmed by subtracting the background signal (PBS only) from the dopamine signal (Fig. 4a inset). These peak potentials are different from those reported in other electroanalytical studies of dopamine,[13,14] likely caused by electrode material differences (*i.e.*, ITO *vs.* ITO here, carbon fiber *vs.* Ag/AgCl in other studies[13,14]). Since the peak at 0.3 V is poorly resolved, the peak at 0.72 V was chosen for quantitative analysis. Fig. 4b shows that the CVs demonstrate consistent behavior across a wide concentration range, and Fig. 4c indicates a linear trend with respect to concentration ($y = 4.145x + 1.570$, $R^2 = 0.9949$), with a limit of detection of LOD = 30 nM (better than 10× improved relative to the LOD = 420 nM for dopamine analysis by DMF/electroanalysis reported previously[33]).

Dopaminergic neuron culture and DA uptake

Armed with a capable DA sensor, we turned to the other goal of this work, on-chip neuron culture and analysis. In initial work, it was determined that the previous methods reported for adherent cell culture in DMF[17–23] were inadequate for the delicate task of growing and differentiating neuronal cells.

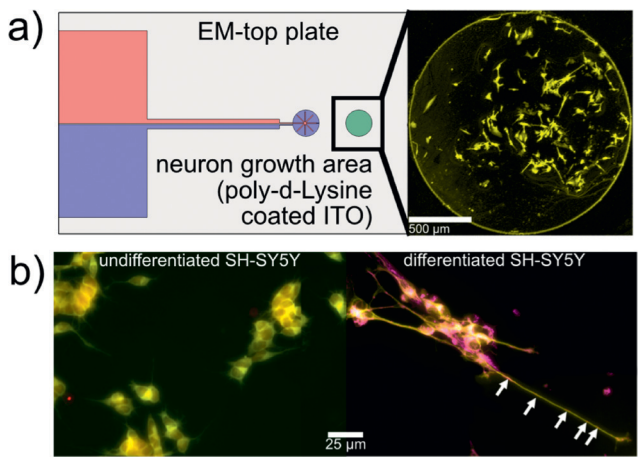

Fig. 5 Neuron differentiation by DMF. a) Top view schematic of EM-top plate (left). Cell culture areas (green) are coated with poly-D-lysine (necessary for neuron attachment, growth and differentiation) and are located adjacent to the electroanalytical cell (WE, red; CE/RE, blue). Fluorescent micrograph (right) of an entire growth area (10× mag.) of day-6 SH-SY5Y cells grown and differentiated by DMF on an EM-top plate. Cells were stained for neuronal structural marker, β_3-tubulin (yellow); the extended neurites are consistent with differentiated SH-SY5Y cell morphology. Scale bar is 500 μm. b) Fluorescent micrographs (40× mag.) of undifferentiated day-1 SH-SY5Y neurons (left) stained for β_3-tubulin (yellow) and day-6 differentiated SH-SY5Y neurons (right) stained for β_3-tubulin (yellow) and mitochondria (pink). Compared with undifferentiated SH-SY5Y cells, the differentiated cells have longer, thicker, and more pronounced neurites. Arrows show mitochondrial migration into a developing neurite, a marker of healthy, active neurons. Scale bar is 25 μm.

Building from well-plate techniques,[10,41,42] we found that coating cell culture sites with PDL (Fig. 5a), allows for neurons to attach and thrive. We optimized the PDL coating conditions for maximum cell attachment and differentiation (data not shown), and obtained mature dopaminergic neurons by seeding immature SH-SY5Y cells on PDL coated liftoff spots, followed by a 6 day differentiation protocol (adapted from one reported elsewhere[10]) in which cells are first exposed to RA and then to TPA (in this case, all automated by DMF). A representative image of undifferentiated cells (Fig. 5b, left) features cells with short, thin neurites, consistent with an immature neuron phenotype. In contrast, terminally differentiated neurons (Fig. 5b, right) show a phenotype consistent with neurons, with β_3-tubulin staining (a marker for neuronal cytoskeleton,[43] in yellow), and mitochondria distribution in the neurites, (denoting active transport, a marker of neuron health,[44] in pink). On average, the main neurites observed in day-6 (terminally) differentiated cells grew ~15-fold relative to basal lengths on day 0; this stands in contrast to those in day-6 undifferentiated cells, which did not grow relative to basal lengths (Fig. S2 in the ESI†). After optimization of the differentiation conditions, a series of virtual microwells ($n = 15$) bearing terminally differentiated SH-SY5Y cells was found to support 209 ± 17 cells, each of which contained 833 ± 63 pg total protein (mean ± S.D.).

As far as we are aware, the data shown here represent the first report of neurons grown on a digital microfluidic platform. Although not evaluated specifically, the process of droplet movement (either to seed suspended cells or deliver reagents to adhered cells) does not appear to affect cell viability or phenotype. This is not surprising, as previous studies on other mammalian cell types[20] have reported that DMF actuation has negligible effects on cell phenotype when probed for targeted (quantitative PCR for stress-related genes) and untargeted (cDNA microarrays) expression changes (noting that DMF driving potentials drop almost exclusively across the dielectric layer, leaving droplets largely field-free). While differentiated SH-SY5Y cells have been grown in microchannel-based platforms,[31] we propose that the low shear stresses inherent to DMF (*e.g.*, 0.5 dyn cm^{-2} even with high-speed solution transfer[22]) makes DMF an attractive platform for neuron growth and analysis applications, given the sensitivity of neurons to modest shear forces (*i.e.*, DNA damage at 1 dyn cm^{-2} or more[45]).

Finally, equipped with a device capable of (a) multiday neuron culture and differentiation and (b) electroanalysis of dopamine in solution, the two functions were integrated into an uninterrupted process-flow, as illustrated in Fig. 6a. In each experiment, after on-chip culture and differentiation for 6 days, the culture/differentiation medium in a virtual microwell (highlighted for clarity with yellow dye) is exchanged with a droplet of PBS containing 1 μM dopamine (highlighted for clarity with green dye) (frames i–iii). After a suitable incubation step, a second droplet is delivered to collect the contents of the virtual microwell and deliver it to the voltammetric sensor (frames iv–vi). The total elapsed time

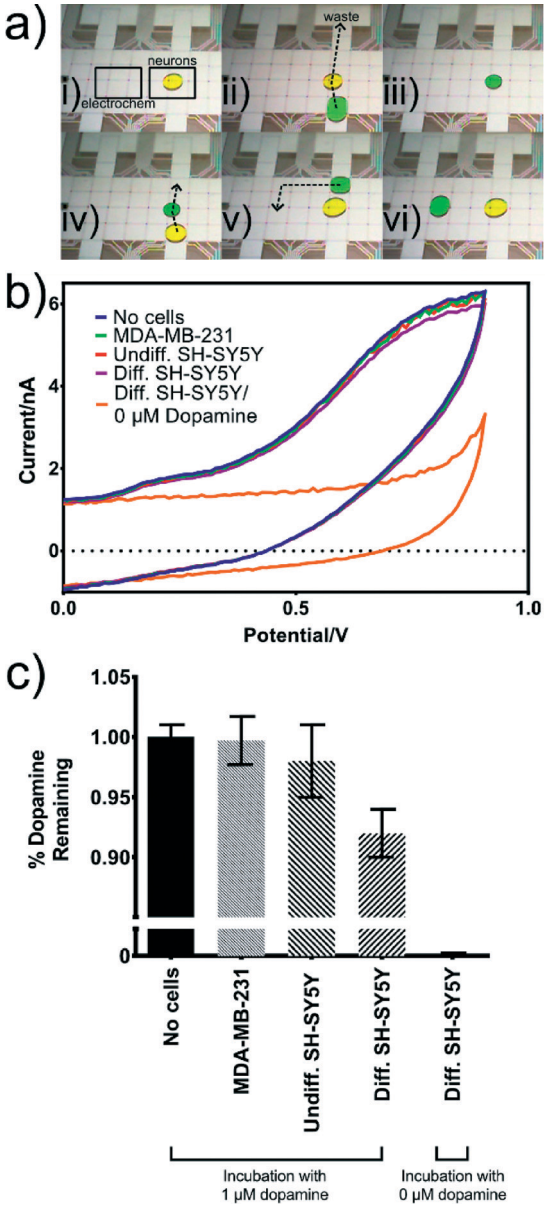

Fig. 6 DMF dopamine uptake assay. a) Frames from a movie showing the assay protocol, with neuron differentiation medium identified by yellow dye, and 1 μM dopamine in 1× PBS identified in green dye. i) A virtual microwell containing adherent neurons is shown on the right, and a (transparent) electroanalytical cell is indicated on the left. ii) The initial differentiation medium on the neurons is replaced with dopamine solution, and iii) the neurons are incubated with dopamine solution. iv) The dopamine solution is replaced with media to maintain neuron viability. v) The spent dopamine solution is collected and vi) is moved to the electroanalytical cell for analysis. b) Representative cyclic voltammograms generated from droplets of 1 μM dopamine after incubation for 10 min over an empty microwell (blue), MDA-MB-231 cells (green), undifferentiated SH-SY5Y cells (pink), and differentiated SH-SY5Y cells (purple). As positive control, a droplet of buffer containing no dopamine was incubated over differentiated SH-SY5Y cells (orange). c) Bar graph comparing the percentage of dopamine remaining in 1 μM dopamine droplets (determined from cyclic voltammetry) after incubating on virtual microwells with (left-to-right) no cells, MDA-MB-231 cells, undifferentiated SH-SY5Y cells, and differentiated SH-SY5Y cells. The final condition (right-most) is for droplets containing no dopamine exposed to differentiated SH-SY5Y cells. Error bars represent ±1 S.D. for n = 10.

between the two steps (incubation and analysis) is short (<5 s), limiting the potential for unwanted DA oxidation. Note that the analyte collection step (frames iv–vi) is not 100% efficient – that is, a small amount of analyte remains in a VM after a single unit droplet is driven across it. To account for this effect, experiments were carried out to determine that the transfer efficiency for the procedure used here is 85% (Fig. S3 in the ESI†), a property that was accounted for in dopamine uptake calculations, below.

Fig. 6b shows representative cyclic voltammograms (CVs) of 1 μM dopamine solutions processed as in Fig. 6a with in-line incubation for 10 min with differentiated SH-SY5Y cells, undifferentiated SH-SY5Y cells, MDA-MB-231 cells (a non-neuronal cell type, included as an organic negative control), and with PDL-coated regions containing no cells (inorganic negative control). In addition, a CV is shown for a droplet containing no dopamine incubated for 10 min with differentiated SH-SY5Y cells (positive control). It is evident that these signals are noisier than those generated from standard solutions (Fig. 4a and b), likely caused by interference of proteins or other solution constituents secreted by cells during the incubation step. Importantly, the shape and magnitude of the CV for the positive control (differentiated SH-SY5Y cells exposed to no dopamine, orange trace in Fig. 6b) is nearly identical to that of the standard solution containing no dopamine (purple trace in Fig. 4b), suggesting that the cells have not secreted appreciable dopamine or other analytes with similar oxidation potentials (*e.g.* norepinephrine) that might obscure the measurement of dopamine uptake.

Ten replicates of each condition represented in Fig. 6b were conducted using the procedure outlined in Fig. 6a, and the results are summarized in Fig. 6c. As shown, the average dopamine signal measured in droplets after exposure to differentiated SH-SY5Y cells is ~8% lower than that measured for the inorganic control. This signal is significantly different than that measured for undifferentiated SH-SY5Y cells (p = 0.0059), and the post-incubation dopamine signals for undifferentiated SH-SY5Y and non-neuronal MDA-MB-231 cells are similar (p = 0.3225). Accounting for the 85% transfer efficiency described above (which applies to all conditions in Fig. 6c), the amount of dopamine taken up by differentiated SH-SY5Y cells is ~32 fmol per VM. This is equivalent to 184 pmol dopamine per mg cellular protein after 10 min exposure to 1 μM dopamine, a rate that is ~4× higher than what was reported for these cells previously.[10] This level of difference is perhaps not surprising given the radically different techniques employed (direct radiometric analysis of [^{3}H]DA in tens of millions of cells previously[10] *vs.* electrochemical analysis of unlabeled DA remaining in supernatant exposed to hundreds of cells here). More tests are needed to know for sure, but it is possible that the higher uptake rates measured here are reflective of the rapid, integrated protocol, which limits the opportunity for dopamine oxidation.

The data presented in Fig. 6 was collected using the first method (of any kind) we are aware of that is capable of automated neuron culture with in-line neurotransmitter

quantitation (and further, the first digital microfluidic method integrating cell culture of any kind with chemical sensors). In this proof-of-principle work, we evaluated one concentration of dopamine at one duration. But we propose that future generations of similar devices (perhaps enabled by recent reports of DMF arrays bearing thousands of driving electrodes[46]) will be useful for multiplexed analysis of dopamine uptake (perhaps with primary neurons or differentiated neurons formed from stem cells[47] rather than the SH-SY5Y cells used here), which would be invaluable for drug discovery for PD and other DA-related neurodegenerative diseases.[1,2] More generally, we propose that the techniques described here will be applicable to a wide range of problems that would benefit from miniaturized, automated techniques that couple cell culture with electroanalysis.

Conclusion

We demonstrate the first integrated in-line detection system to study dopamine uptake. The method relies on digital microfluidics and combines 1) multi-day, *in vitro* culture and differentiation of neurons, and 2) a sensitive electrochemical sensor for neurotransmitter detection. The system allows for integrated dopamine uptake assays in an automated format suitable for screening. We propose that future generations of this platform will be useful to study a number of neuropathologies, as well as applications involving other electroactive neurotransmitters and their associated transporters.

Acknowledgements

We thank the Canadian Institutes for Health Research (CIHR) and the Ontario Research Foundation (ORF) for support. We thank Ian Swyer and Prof. Kagan Kerman (both at Univ. Toronto) for valuable discussions regarding the electrochemical sensor and simulations. A. R. W. thanks the Canada Research Chair (CRC) Program for a CRC.

References

1 D. Sakrikar, M. S. Mazei-Robison, M. A. Mergy, N. W. Richtand, Q. Han, P. J. Hamilton, E. Bowton, A. Galli, J. Veenstra-Vanderweele and M. Gill, Attention Deficit/Hyperactivity Disorder-Derived Coding Variation In The Dopamine Transporter Disrupts Microdomain Targeting And Trafficking Regulation, *J. Neurosci.*, 2012, **32**, 5385–5397.

2 R. A. Vaughan and J. D. Foster, Mechanisms Of Dopamine Transporter Regulation In Normal And Disease States, *Trends Pharmacol. Sci.*, 2013, **34**, 489–496.

3 A. Bellucci, M. Zaltieri, L. Navarria, J. Grigoletto, C. Missale and P. Spano, From Alpha-Synuclein To Synaptic Dysfunctions: New Insights Into The Pathophysiology Of Parkinson's Disease, *Brain Res.*, 2012, **1476**, 183–202.

4 H. Jiang, Q. Jiang and J. Feng, Parkin Increases Dopamine Uptake By Enhancing The Cell Surface Expression Of Dopamine Transporter, *J. Biol. Chem.*, 2004, **279**, 54380–54386.

5 A. W. Oaks and A. Sidhu, Synuclein Modulation Of Monoamine Transporters, *FEBS Lett.*, 2011, **585**, 1001–1006.

6 J. Swant, J. S. Goodwin, A. North, A. A. Ali, J. Gamble-George, S. Chirwa and H. Khoshbouei, Alpha-Synuclein Stimulates A Dopamine Transporter-Dependent Chloride Current And Modulates The Activity Of The Transporter, *J. Biol. Chem.*, 2011, **286**, 43933–43943.

7 J. Eriksen, T. N. Jorgensen and U. Gether, Regulation Of Dopamine Transporter Function By Protein-Protein Interactions: New Discoveries And Methodological Challenges, *J. Neurochem.*, 2010, **113**, 27–41.

8 J. D. Foster and R. A. Vaughan, Palmitoylation Controls Dopamine Transporter Kinetics, Degradation, And Protein Kinase C-Dependent Regulation, *J. Biol. Chem.*, 2011, **286**, 5175–5186.

9 J. D. Foster, J. W. Yang, A. E. Moritz, S. Challasivakanaka, M. A. Smith, M. Holy, K. Wilebski, H. H. Sitte and R. A. Vaughan, Dopamine Transporter Phosphorylation Site Threonine 53 Regulates Substrate Reuptake And Amphetamine-Stimulated Efflux, *J. Biol. Chem.*, 2012, **287**, 29702–29712.

10 S. P. Presgraves, T. Ahmed, S. Borwege and J. N. Joyce, Terminally Differentiated Sh-Sy5y Cells Provide A Model System For Studying Neuroprotective Effects Of Dopamine Agonists, *Neurotoxic. Res.*, 2003, **5**, 579–598.

11 A. Klegeris, L. G. Korkina and S. A. Greenfield, Autoxidation Of Dopamine: A Comparison Of Luminescent And Spectrophotometric Detection In Basic Solutions, *Free Radical Biol. Med.*, 1995, **18**, 215–222.

12 C. C. Chiueh, G. Krishna, P. Tulsi, T. Obata, K. Lang, S.-J. Huang and D. L. Murphy, Intracranial Microdialysis Of Salicylic Acid To Detect Hydroxyl Radical Generation Through Dopamine Autooxidation In The Caudate Nucleus: Effects Of Mpp+, *Free Radical Biol. Med.*, 1992, **13**, 581–583.

13 C. M. Cameron, R. M. Wightman and R. M. Carelli, Dynamics Of Rapid Dopamine Release In The Nucleus Accumbens During Goal-Directed Behaviors For Cocaine Versus Natural Rewards, *Neuropharmacology*, 2014, **86**, 319–328.

14 P. E. Phillips, G. D. Stuber, M. L. Heien, R. M. Wightman and R. M. Carelli, Subsecond Dopamine Release Promotes Cocaine Seeking, *Nature*, 2003, **422**, 614–618.

15 K. Choi, A. H. Ng, R. Fobel and A. R. Wheeler, Digital Microfluidics, *Annu. Rev. Anal. Chem.*, 2012, **5**, 413–440.

16 A. H. Ng, B. B. Li, M. D. Chamberlain and A. R. Wheeler, Digital Microfluidic Cell Culture, *Annu. Rev. Biomed. Eng.*, 2015, **17**, 91–112.

17 D. Bogojevic, M. D. Chamberlain, I. Barbulovic-Nad and A. R. Wheeler, A Digital Microfluidic Method For Multiplexed Cell-Based Apoptosis Assays, *Lab Chip*, 2012, **12**, 627–634.

18 S. Srigunapalan, I. A. Eydelnant, C. A. Simmons and A. R. Wheeler, A Digital Microfluidic Platform For Primary Cell Culture And Analysis, *Lab Chip*, 2012, **12**, 369–375.

19 S. C. C. Shih, I. Barbulovic-Nad, X. Yang, R. Fobel and A. R. Wheeler, Digital Microfluidics With Impedance Sensing For

Integrated Cell Culture And analysis, *Biosens. Bioelectron.*, 2013, **42**, 314–320.

20 S. H. Au, R. Fobel, S. P. Desai, J. Voldman and A. R. Wheeler, Cellular Bias On The Microscale: Probing The Effects Of Digital Microfluidic Actuation On Mammalian Cell Health, Fitness And Phenotype, *Integr. Biol.*, 2013, **5**, 1014–1025.

21 I. A. Eydelnant, U. Uddayasankar, M. W. Liao and A. R. Wheeler, Virtual Microwells For Digital Microfluidic Reagent Dispensing And Cell Culture, *Lab Chip*, 2012, **12**, 750–757.

22 A. H. Ng, M. D. Chamberlain, H. Situ, V. Lee and A. R. Wheeler, Digital Microfluidic Immunocytochemistry In Single Cells, *Nat. Commun.*, 2015, **6**, 7513.

23 D. Witters, N. Vergauwe, S. Vermeir, F. Ceyssens, S. Liekens, R. Puers and J. Lammertyn, Biofunctionalization Of Electrowetting-On-Dielectric Digital Microfluidic Chips For Miniaturized Cell-Based Applications, *Lab Chip*, 2011, **11**, 2790–2794.

24 A. M. Taylor, M. Blurton-Jones, S. W. Rhee, D. H. Cribbs, C. W. Cotman and N. L. Jeon, A Microfluidic Culture Platform For Cns Axonal Injury, Regeneration And Transport, *Nat. Methods*, 2005, **2**, 599–605.

25 T. Honegger, M. A. Scott, M. F. Yanik and J. Voldman, Electrokinetic Confinement Of Axonal Growth For Dynamically Configurable Neural Networks, *Lab Chip*, 2013, **13**, 589–598.

26 H. Lu, L. Y. Koo, W. M. Wang, D. A. Lauffenburger, L. G. Griffith and K. F. Jensen, Microfluidic Shear Devices For Quantitative Analysis Of Cell Adhesion, *Anal. Chem.*, 2004, **76**, 5257–5264.

27 M. Zhong, C. Y. Lee, C. A. Croushore and J. V. Sweedler, Label-Free Quantitation Of Peptide Release From Neurons In A Microfluidic Device With Mass Spectrometry Imaging, *Lab Chip*, 2012, **12**, 2037–2045.

28 L. J. Millet, M. E. Stewart, J. V. Sweedler, R. G. Nuzzo and M. U. Gillette, Microfluidic Devices For Culturing Primary Mammalian Neurons At Low Densities, *Lab Chip*, 2007, **7**, 987–994.

29 W. R. Kim, M. J. Jang, S. Joo, W. Sun and Y. Nam, Surface-Printed Microdot Array Chips For The Quantification Of Axonal Collateral Branching Of A Single Neuron In Vitro, *Lab Chip*, 2014, **14**, 799–805.

30 S. Joo, K. Kang and Y. Nam, In Vitro Neurite Guidance Effects Induced By Polylysine Pinstripe Micropatterns With Polylysine Background, *J. Biomed. Mater. Res., Part A*, 2015, **103**, 2731–2739.

31 N.-D. Dinh, Y.-Y. Chiang, H. Hardelauf, J. Baumann, E. Jackson, S. Waide, J. Sisnaiske, J.-P. Frimat, C. Van Thriel and D. Janasek, Microfluidic Construction Of Minimalistic Neuronal Co-Cultures, *Lab Chip*, 2013, **13**, 1402–1412.

32 M. H. Shamsi, K. Choi, A. H. Ng and A. R. Wheeler, A Digital Microfluidic Electrochemical Immunoassay, *Lab Chip*, 2014, **14**, 547–554.

33 Y. Yu, J. Chen and J. Zhou, Parallel-Plate Lab-On-A-Chip Based On Digital Microfluidics For On-Chip Electrochemical Analysis, *J. Micromech. Microeng.*, 2014, **24**, 015020.

34 M. D. Dryden, D. D. Rackus, M. H. Shamsi and A. R. Wheeler, Integrated Digital Microfluidic Platform For Voltammetric Analysis, *Anal. Chem.*, 2013, **85**, 8809–8816.

35 D. G. Rackus, M. D. M. Dryden, J. Lamanna, A. Zaragoza, B. Lam, S. O. Kelley and A. R. Wheeler, A Digital Microfluidic Device With Integrated Nanostructured Microelectrodes For Electrochemical Immunoassays, *Lab Chip*, 2015, **15**, 3776–3784.

36 M. D. M. Dryden and A. R. Wheeler, Dstat: A Versatile, Open-Source Potentiostat For Electroanalysis And Integration, *PLoS One*, 2015, **10**, E0140349.

37 A. H. Ng, K. Choi, R. P. Luoma, J. M. Robinson and A. R. Wheeler, Digital Microfluidic Magnetic Separation For Particle-Based Immunoassays, *Anal. Chem.*, 2012, **84**, 8805–8812.

38 R. Fobel, C. Fobel and A. R. Wheeler, Dropbot: An Open-Source Digital Microfluidic Control System With Precise Control Of Electrostatic Driving Force And Instantaneous Drop Velocity Measurement, *Appl. Phys. Lett.*, 2013, **102**, 193513.

39 A. J. Bard and L. R. Faulkner, *Electrochemical Methods: Fundamentals And Applications, 2nd Edition*, John Wiley And Sons Publishers, 2nd edn, 2001.

40 R. N. Goyal, V. K. Gupta, M. Oyama and N. Bachheti, Gold Nanoparticles Modified Indium Tin Oxide Electrode For The Simultaneous Determination Of Dopamine And Serotonin: Application In Pharmaceutical Formulations And Biological Fluids, *Talanta*, 2007, **72**, 976–983.

41 R. Constantinescu, A. Constantinescu, H. Reichmann and B. Janetzky, *Neuronal Differentiation And Long-Term Culture Of The Human Neuroblastoma Line Sh-Sy5y*, Springer, 2007.

42 J. Jordán, M. F. Galindo, D. Tornero, C. González-García and V. Ceña, Bcl-Xl Blocks Mitochondrial Multiple Conductance Channel Activation And Inhibits 6-Ohda-Induced Death In Sh-Sy5y Cells, *J. Neurochem.*, 2004, **89**, 124–133.

43 K. F. Sullivan and D. W. Cleveland, Identification Of Conserved Isotype-Defining Variable Region Sequences For Four Vertebrate Beta Tubulin Polypeptide Classes, *Proc. Natl. Acad. Sci. U. S. A.*, 1986, **83**, 4327–4331.

44 T. L. Schwarz, Mitochondrial Trafficking In Neurons, *Cold Spring Harbor Perspect. Biol.*, 2013, **5**, a011304.

45 M. E. Edwards, S. S. S. Wang and T. A. Good, Role Of Viscoelastic Properties Of Differentiated Sh-Sy5y Human Neuroblastoma Cells In Cyclic Shear Stress Injury, *Biotechnol. Prog.*, 2001, **17**, 760–767.

46 B. Hadwen, G. Broder, D. Morganti, A. Jacobs, C. Brown, J. Hector, Y. Kubota and H. Morgan, Programmable Large Area Digital Microfluidic Array With Integrated Droplet Sensing For Bioassays, *Lab Chip*, 2012, **12**, 3305–3313.

47 M. Robinson, S.-Y. Yau, L. Sun, N. Gabers, E. Bibault, B. R. Christie and S. M. Willerth, Optimizing Differentiation Protocols For Producing Dopaminergic Neurons From Human Induced Pluripotent Stem Cells For Tissue Engineering Applications, *Biomarker Insights*, 2015, **10**(S1), 61–70.

